SINTEF
PROCEEDINGS
2

Proceedings of the 12th International Conference on Computational Fluid Dynamics in the Oil & Gas, Metallurgical and Process Industries

Progress in Applied CFD – CFD2017

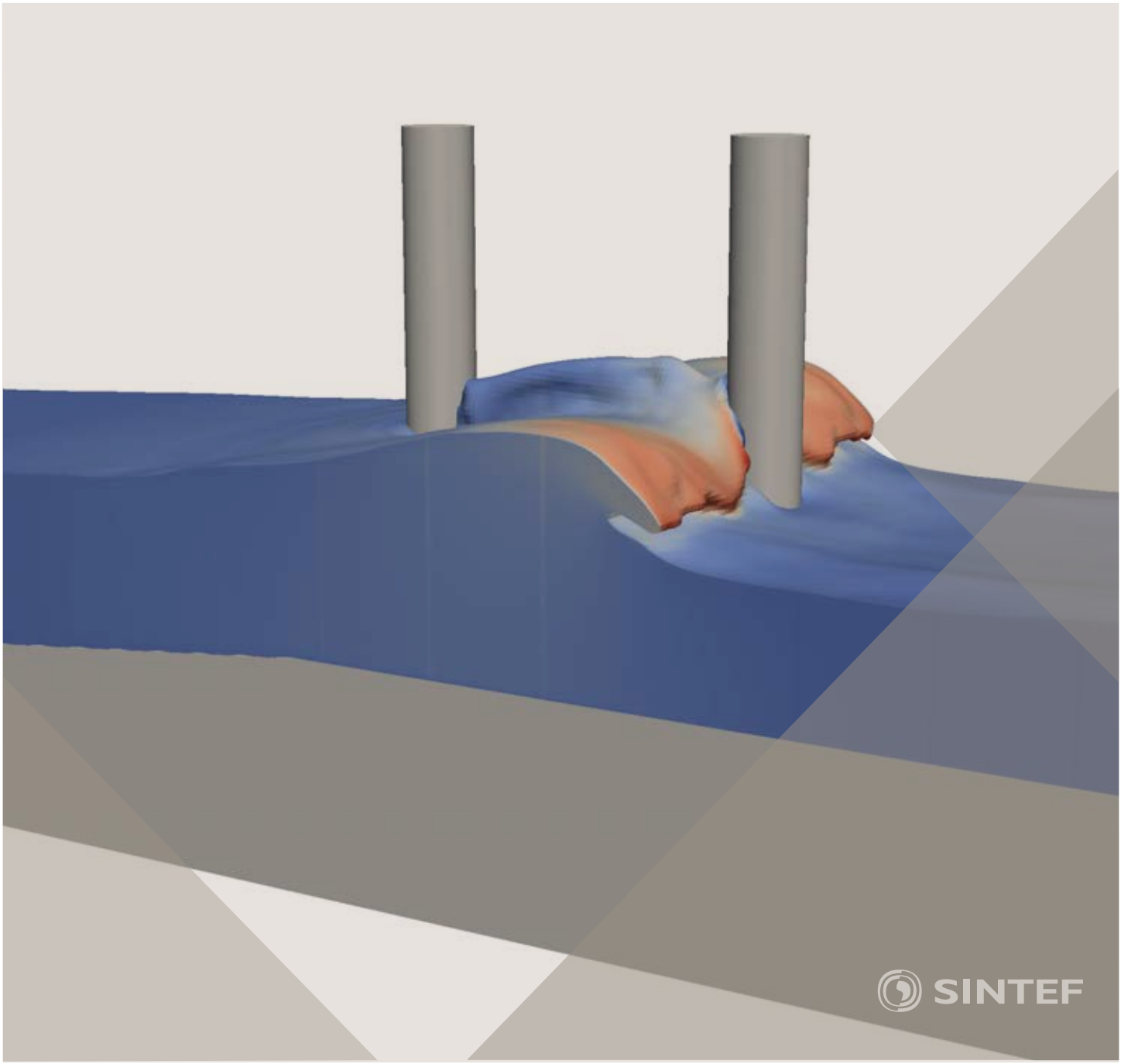

SINTEF Proceedings

Editors:
Jan Erik Olsen and Stein Tore Johansen

Progress in Applied CFD – CFD2017

Proceedings of the 12th International Conference on Computational Fluid Dynamics in the Oil & Gas, Metallurgical and Process Industries

SINTEF Academic Press

SINTEF Proceedings no 2
Editors: Jan Erik Olsen and Stein Tore Johansen
Progress in Applied CFD – CFD2017
Selected papers from 10th International Conference on Computational Fluid Dynamics in the Oil & Gas, Metallurgical and Process Industries

Key words:
CFD, Flow, Modelling

Cover, illustration: Arun Kamath

ISSN 2387-4295 (online)
ISBN 978-82-536-1544-8 (pdf)

SINTEF Academic Press
Address: Forskningsveien 3 B
PO Box 124 Blindern
N-0314 OSLO
Tel: +47 73 59 30 00
Fax: +47 22 96 55 08

www.sintef.no/byggforsk
www.sintefbok.no

SINTEF Proceedings
SINTEF Proceedings is a serial publication for peer-reviewed conference proceedings on a variety of scientific topics.
The processes of peer-reviewing of papers published in SINTEF Proceedings are administered by the conference organizers and proceedings editors. Detailed procedures will vary according to custom and practice in each scientific community.

PREFACE

This book contains all manuscripts approved by the reviewers and the organizing committee of the 12th International Conference on Computational Fluid Dynamics in the Oil & Gas, Metallurgical and Process Industries. The conference was hosted by SINTEF in Trondheim in May/June 2017 and is also known as CFD2017 for short. The conference series was initiated by CSIRO and Phil Schwarz in 1997. So far the conference has been alternating between CSIRO in Melbourne and SINTEF in Trondheim. The conferences focuses on the application of CFD in the oil and gas industries, metal production, mineral processing, power generation, chemicals and other process industries. In addition pragmatic modelling concepts and bio-mechanical applications have become an important part of the conference. The papers in this book demonstrate the current progress in applied CFD.

The conference papers undergo a review process involving two experts. Only papers accepted by the reviewers are included in the proceedings. 108 contributions were presented at the conference together with six keynote presentations. A majority of these contributions are presented by their manuscript in this collection (a few were granted to present without an accompanying manuscript).

The organizing committee would like to thank everyone who has helped with review of manuscripts, all those who helped to promote the conference and all authors who have submitted scientific contributions. We are also grateful for the support from the conference sponsors: ANSYS, SFI Metal Production and NanoSim.

Stein Tore Johansen & Jan Erik Olsen

Organizing committee:

Conference chairman: Prof. Stein Tore Johansen
Conference coordinator: Dr. Jan Erik Olsen
Dr. Bernhard Müller
Dr.Sigrid Karstad Dahl
Dr.Shahriar Amini
Dr.Ernst Meese
Dr.Josip Zoric
Dr.Jannike Solsvik
Dr.Peter Witt

Scientific committee:

Stein Tore Johansen, SINTEF/NTNU
Bernhard Müller, NTNU
Phil Schwarz, CSIRO
Akio Tomiyama, Kobe University
Hans Kuipers, Eindhoven University of Technology
Jinghai Li, Chinese Academy of Science
Markus Braun, Ansys
Simon Lo, CD-adapco
Patrick Segers, Universiteit Gent
Jiyuan Tu, RMIT
Jos Derksen, University of Aberdeen
Dmitry Eskin, Schlumberger-Doll Research
Pär Jönsson, KTH
Stefan Pirker, Johannes Kepler University
Josip Zoric, SINTEF

CONTENTS

A MULTIFLUID-PBE MODEL FOR A SLURRY BUBBLE COLUMN WITH BUBBLE SIZE DEPENDENT VELOCITY, WEIGHT FRACTIONS AND TEMPERATURE

Camilla Berge VIK[1*], **Jannike SOLSVIK**[1†], **Mathias ENGH**[1‡], **Magne HILLESTAD**[1§], **Hugo Atle JAKOBSEN**[1¶]

[1]NTNU Department of Chemical Engineering, 7491 Trondheim, NORWAY

[*] E-mail: camilla.berge.vik@ntnu.no
[†] E-mail: jannike.solsvik@ntnu.no
[‡] E-mail: mathias.engh@ntnu.no
[§] E-mail: magne.hillestad@ntnu.no
[¶] E-mail: hugo.a.jakobsen@ntnu.no

ABSTRACT

With kinetic gas theory as a starting point, equations of change for total mass, species mass, momentum and inner energy are developed for the dispersed gaseous phase and implemented to describe the Fischer-Tropsch synthesis carried out at industrial scale. The resultant model describes bubble velocity, composition and temperature in the gaseous phase as function of axial position and bubble size. The bubble size is found from the population balance equation (PBE) using a continuous mass density function which is calculated explicitly and used as basis for the gas-liquid transfer fluxes of species mass, momentum and heat. In the Fischer-Tropsch synthesis reactants are transported from inside gas bubbles through the gas-liquid interface into the liquid phase and subsequently into the catalyst pores to form hydrocarbon products at the active sites on the catalyst surface. Higher catalyst loading requires a higher mass transfer from the gas bubbles to the liquid phase and may cause the overall reaction to become mass transfer limited. In order to optimize reactor design, knowledge of the bubble size may thus be of importance. The liquid and solid phases are modelled using conventional continuum mechamics equations of change. The results of the simulations show that the weight percent of reactant varies by 20 percentage points from the smallest to the largest bubble size and thus a significant level of detail is added to the model when including bubble size in the mass fraction variable. For temperature the particle size dependency is negligible at the same conditions. It is noted that firm conclusions on the mass and heat transfer limitations can only be drawn when reliable estimates of the transfer coefficients are available.

Keywords: population balance methods, chemical reactors, slurry bubble column, multiphase mass transfer, Fischer-Tropsch synthesis, bubble size .

NOMENCLATURE

Greek Symbols

α	Volume fraction, $[-]$.
γ	Size dependent mass transfer term, $[1/s]$.
γ_s	Size dependent mass transfer term for species s, $[1/s]$.
Γ	Mass transfer term, $[kg/m^3\ s]$.
ζ	Bubble diameter, $[m]$.
λ	Effective turbulent conductivity in spatial space, $[W/m\ K]$.
μ	Dynamic viscosity, $[kg/ms]$.
ξ	Bubble diameter, $[m]$.
Ξ	Microscopical velocity in property space, $[m/s]$.
ρ	Mass density, $[kg/m^3]$.
ρ_{cat}	Catalyst density in reactor, $[kg/m^3]$.
ψ	Generic quantity.
ω	Weight fraction, $[-]$.

Latin Symbols

A	Bubble surface area, $[m^2]$.
a_L	Gas-liquid interfacial area per unit dispersion mixture, $[m^2/m^3]$.
b	Breakage frequency, $[1/s]$.
c	Coalescence frequency, $[1/s]$.
$\boldsymbol{c}$	Microscopical velocity in physical space, $[m/s]$.
C_D	Drag coefficient, $[-]$.
c_p	Specific heat capacity, $[J/kg\ K]$.
d_s	Sauter mean diameter, $[m]$.
D	Diameter of column, $[m]$.
D_{eff}	Eff. axial dispersion coefficient, $[m^2/s]$.
f	Number density function, $[\#/m^3\ m]$.
f_d	Mass density function, $[kg/m^3\ m]$.
f_{drag}	Size dependent drag force per mass, $[N/kg]$.
$\boldsymbol{F}$	Force, $[N]$.
g	Standard acceleration of gravity, $[m/s^2]$.
h	Heat transfer coefficient, $[W/m^2\ K]$.
h	Specific enthalpy, $[J/kg]$.
h_b	Daughter size redistribution function, $[1/m]$.
J	Source term, $[kg/m^3\ s]$.
k_L	Liquid side mass transfer coefficient, $[m/s]$.
K	Equilibrium constant describing the relationship y_i^*/x_i^* at given conditions, $[-]$.
m	Mass, $[kg]$.
p	Microscopical density function, $[\#/(m^3\ m\ m/s\ K\ kg)]$.
P	Microscopical normalized density function, $[\#/(m/s\ K)]$.
p	Pressure, $[Pa]$.
$\boldsymbol{P}$	Pressure tensor, $[kg/m\ s^2]$.
$\boldsymbol{p}_\xi$	Space-property pressure vector, $[kg/m\ s^2]$.
$\boldsymbol{q}$	Kinetic energy flux vector, $[W/m^2]$.
$\boldsymbol{q}_\xi$	Space-property kinetic energy flux vector, $[W/m^2]$.
$\boldsymbol{r}$	Physical coordinates, $[m]$.
r_{CO}	Reaction rate in terms of CO conversion, $[kmol\ s/kgcat]$.
R	Reaction term, $[kg/m^3\ s]$.
S	Source term not due to collisions,
t	Time, $[s]$.
T	Temperature, $[K]$.
v	Velocity, $[m/s]$.
V	Bubble volume, $[m^3]$.

v_ξ Growth velocity, $[m/s]$.
z Dispersion height, $[m]$.

Sub/superscripts
$B-D$ Birth and death terms.
coll Collisions.
d (mass) density function.
eff Effective.
G Gas.
$G-L$ Gas-liquid.
in (Reactor) inlet.
L Liquid.
m Mass.
max Maximum.
min Minimum.
p Particle.
r Physical space.
s Superficial (superscript).
s Chemical species (subscript).
S Solid.
$S-L$ Solid-liquid.
SL Slurry.
z z (axial) direction.
ξ Property space.

INTRODUCTION

Background

In the modelling of multiphase chemical reactors the interfacial transfer fluxes play an important role. Chemical species are transported between the phases to form products, interfacial forces influence the relative velocities of the phases and heat is transfered from one phase to another. Mathematical models for reactive *dispersed* flows (as opposed to *stratified*) are developed on basis of continuum mechanics and kinetic theory of gases (Jakobsen, 2008). With emphasis on modelling the interfacial transfer fluxes, the latter framework is of interest as it provides a density function describing the number of entities at a location in physical space and property space. Solving for the density function explicitly, the transfer of chemical species, momentum and heat can thus be calculated as the product of the transfer coefficient, the density function and a property dependent driving force. In particular, choosing size (diameter) as the property space / inner coordinate the influence of the bubble size distribution on mass, momentum and heat transfer can be studied.

Development of a reactive multifluid-PBE model

A multifluid-PBE model, where PBE denotes the population balance equation, was developed by Dorao (2006), Zhu (2009), Patruno *et al.* (2009), Sporleder (2011), Nayak *et al.* (2011) and Solsvik and Jakobsen (2014) to describe isothermal non-reactive flow with size dependent velocity. Based on the works by Andresen (1990) and Simonin (1996) a model for reactive, non-isothermal solid particles in gas was developed by Lathouwers and Bellan (2000) to describe the gasification of biomass. Chao (2012) extended their model to allow for two types of particles in a gas and applied it to sorption enhanced steam methane reforming. With the kinetic theory of gases in common, this work extends the above models to describe reactive, non-isothermal gas bubbles in a liquid phase with size dependent velocity, weight fractions and temperature. An explicit and continous mass density function describes the mass of bubbles at a point in physical space z (axial direction) and property space ξ (diameter).

Application of the multifluid-PBE to the Fischer-Tropsch synthesis

The multifluid-PBE model is applied to the Fischer-Tropsch synthesis of liquid hydrocarbons from biomass carbon sources, termed Biomass-to-Liquid (BtL). Torrefication and gasification of wood residue such as branches and tops gives synthesis gas which is fed to a reactor where it is converted to hydrocarbons over a catalyst.
A potential reactor for this process is the slurry bubble column (Figure 1) where the reactants are fed as gas through a slurry composed of solid catalyst submerged in a liquid phase. In order to form products, carbon monoxide and hydrogen are transported from the gas bubbles to the liquid phase and into the catalyst pores where they form hydrocarbons of various lengths in a very exothermal reaction. With high gas flow rates and the requirement of efficient mass transfer and heat removal the Fischer-Tropsch process requires accurate description of size dependent interfacial transfer fluxes and field variables such as weight fraction, velocity and temperature.

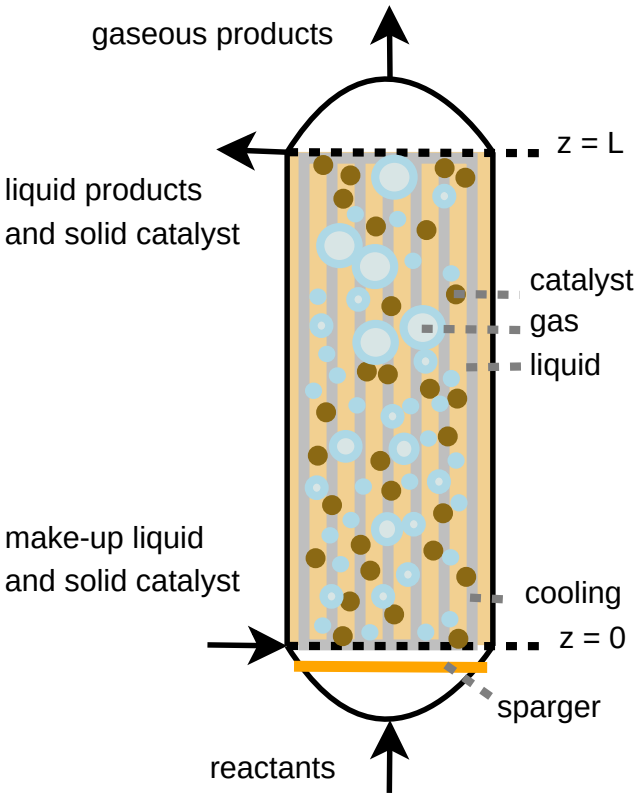

Figure 1: Slurry bubble column reactor for the Fischer-Tropsch synthesis. Solid catalyst is submerged in the liquid phase. Gas bubbles with reactant are injected through a sparger. Cooling rods along the axial direction facilitate removal of reaction heat from the liquid phase.

Mass transfer

Efficient mass transfer of reactants from gas phase to liquid phase along with fast reaction kinetics are important for the overall reactor efficiency for the Fischer-Tropsch synthesis in a slurry bubble column. In this work, the kinetic model by Yates and Satterfield (1991) is applied to study the conversion of reactants and a standard Anderson-Schultz-Flory distribution is applied to estimate the chain length of the hydrocarbon products.

A schematic view of the mass transfer resistances in the Fischer-Tropsch synthesis in a slurry bubble column is shown in Figure 2. It is known that among all the mass transfer resistances from gas bubble to inside the catalyst pellet the liquid side mass transfer is the limiting (Kohler, 1986). Values for the liquid side mass transfer coefficient for Fischer-Tropsch fluids vary by an order of magnitude (Vandu *et al.*, 2004). In this work the model by Calderbank and Moo-Young (1961) for small bubbles is applied. While the authors denoted small bubbles as those with diameter less than 2.5 mm, they remarked that most industrial reactors exhibit conditions where the small bubble correlation was better than their large bubble correlation.

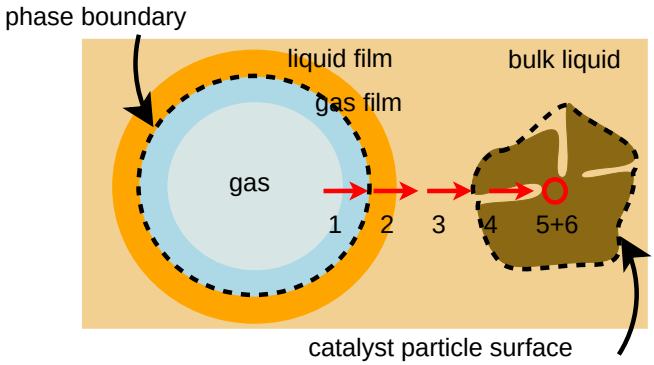

Figure 2: Possible mass transfer limitations (Kohler, 1986), whereas step (2) is the most important.

Momentum transfer

The main momentum transfer is the drag force between the gas bubbles and the liquid phase. The gas bubbles are fed at a velocity of 0.5 m/s while the liquid phase initial velocity is 0.02 m/s, thus the drag force is significant. Bubble size dependent velocity is known from the literature to give a valuable additional information compared to all bubbles having the same average velocity (e.g. Frank *et al.* (2005)). As shown before for the Fischer-Tropsch synthesis in a slurry bubble column (Vik *et al.*, 2015) the velocity varies significantly with bubble size - mainly as a result of the drag force dependency on bubble size.

Heat transfer

The interfacial gas-liquid heat flux is modelled using the heat transfer coefficient by Calderbank and Moo-Young (1961). The reaction heat is removed from the liquid using axial cooling rods. In this work we have assumed only the liquid phase to be in contact with the axial cooling rods (See Figure 1) and thus only the gas-liquid interfacial heat transfer is relevant for the bubble size dependent gas temperature.

THEORY

The Boltzmann equation

An analogy to the kinetic theory of granular flow is applied to describe reactive bubbles in an interstitial liquid. The starting point is a microscopical density function $p = p(\boldsymbol{r},\xi,\boldsymbol{c},\Xi,\omega_{s,p},T_p,m_p,t)$ which describes the number of bubbles located at point $\boldsymbol{r}$ with size ξ, physical velocity $\boldsymbol{c}$, property velocity (growth) Ξ, weight fraction of species s $\omega_{s,p}$, temperature T_p, mass m_p at time t. Compared to the model of Lathouwers and Bellan (2000)/ Chao (2012) the coordinate set is extended to include the size in form of the diameter ξ and velocity in diameter; growth Ξ. A Boltzmann-like equation for p is formulated as

$$\begin{aligned}&\frac{\partial p}{\partial t}+\boldsymbol{c}\cdot\frac{\partial p}{\partial \boldsymbol{r}}+\boldsymbol{F}\cdot\frac{\partial p}{\partial \boldsymbol{c}}+\Xi\frac{\partial p}{\partial \xi}+F_\xi\frac{\partial p}{\partial \Xi}+\dot{T}_p\frac{\partial p}{\partial T_p}\\&+\sum_s\dot{\omega}_{s,p}\frac{\partial p}{\partial \omega_{s,p}}+\dot{m}_p\frac{\partial p}{\partial m_p}=\left(\frac{\partial p}{\partial t}\right)_{\text{collision}}+S\end{aligned}\tag{1}$$

The two terms on the right hand side denote the changes in p due to collision events and other (not collision) events. Equation 1 is multiplied with a microscopical quantity ψ_p and the mass m_p and then integrated. Lathouwers and Bellan (2000) multiplied with the particle mass and integrated over the entire space except physical location and time. Nayak *et al.* (2011) assumed constant particle mass and integrated over the entire space except physical location, size and time. We here multiply with particle mass and integrate over the entire space except physical location, size and time. This gives a mass averaged momentum equation:

$$\begin{aligned}&\frac{\partial}{\partial t}(f_d\langle\psi_p\rangle)+\frac{\partial}{\partial \boldsymbol{r}}\cdot(f_d\langle\psi_p\boldsymbol{c}\rangle)+\frac{\partial}{\partial \xi}(f_d\langle\Xi\psi_p\rangle)=\\&f_d\left[\langle\frac{\partial\psi_p}{\partial t}\rangle+\langle\boldsymbol{c}\cdot\frac{\partial\psi_p}{\partial \boldsymbol{r}}\rangle+\langle\boldsymbol{F_r}\cdot\frac{\partial\psi_p}{\partial \boldsymbol{c}}\rangle+\langle\Xi\frac{\partial\psi_p}{\partial \xi}\rangle\right]\\&+f_d\left[\langle F_\xi\frac{\partial\psi_p}{\partial \Xi}\rangle+\langle\dot{T}_p\frac{\partial\psi_p}{\partial T_p}\rangle+\sum_s\langle\dot{\omega}_{s,p}\frac{\partial\psi_p}{\partial\omega_{s,p}}\rangle\right]\\&+f_d\left[\langle\dot{m}_p\left(\frac{\partial\psi_p}{\partial m_p}+\frac{1}{m_p}\right)\rangle\right]+\langle J_{\psi_p}\rangle\end{aligned}\tag{2}$$

Equations of change for the dispersed fluid are found by introducing appropriate quantities for ψ_p. We shall introduce *coordinates* for ψ_p thus using an Eulerian framework.

Definitions

We define an average of the macroscopical number density:

$$f(\boldsymbol{r},\xi,t)=\int_{-\infty}^{+\infty}p(\boldsymbol{r},\xi,\boldsymbol{c},\Xi,\omega_{s,p},T_p,m_p,t)d\boldsymbol{c}d\Xi d\omega_{s,p}dT_pdm_p\tag{3}$$

and mass density:

$$f_d(\boldsymbol{r},\xi,t)=\int_{-\infty}^{+\infty}m_pp(\boldsymbol{r},\xi,\boldsymbol{c},\Xi,\omega_{s,p},T_p,m_p,t)d\Omega\tag{4}$$

where $d\Omega = d\boldsymbol{c}d\Xi d\omega_{s,p}dT_pdm_p$ for brevity. Fluid properties are found from moments of ψ_p, defined as:

$$\langle\psi_p\rangle=\int_{-\infty}^{+\infty}\psi_pm_pP(\boldsymbol{r},\xi,\boldsymbol{c},\Xi,\omega_{s,p},T_p,m_p,t)d\Omega\tag{5}$$

where $P(\boldsymbol{r},\xi,\boldsymbol{c},\Xi,\omega_{s,p},T_p,m_p,t)$ is a normalized microscopical density function, defined as:

$$P(\boldsymbol{r},\xi,\boldsymbol{c},\Xi,\omega_{s,p},T_p,m_p,t)=\frac{p(\boldsymbol{r},\xi,\boldsymbol{c},\Xi,\omega_{s,p},T_p,m_p,t)}{f_d(\boldsymbol{r},\xi,t)}\tag{6}$$

This yields and alternative formulation of the moment:

$$\begin{aligned}\langle\psi_p\rangle&=\int_{-\infty}^{+\infty}\psi_pm_p\frac{p(\boldsymbol{r},\xi,\boldsymbol{c},\Xi,\omega_{s,p},T_p,m_p,t)}{f_d(\boldsymbol{r},\xi,t)}d\Omega\\&=\frac{1}{f_d(\boldsymbol{r},\xi,t)}\int_{-\infty}^{+\infty}\psi_pm_ppd\Omega\end{aligned}\tag{7}$$

Average, or macroscopical bubble mass is found by:

$$m(\boldsymbol{r},\xi,t)=\langle m_p\rangle=\frac{1}{f_d(\boldsymbol{r},\xi,t)}\int_{-\infty}^{+\infty}m_pm_ppd\Omega\tag{8}$$

and we adopt the relation:

$$f_d(\boldsymbol{r},\xi,t) = f(\boldsymbol{r},\xi,t)m(\boldsymbol{r},\xi,t) \tag{9}$$

from Lathouwers and Bellan (2000). Macroscopical or average dispersed fluid properties such as velocity, growth velocity, weight fraction of species s, temperature and enthalpy are then given as:

$$\boldsymbol{v_r}(\boldsymbol{r},\xi,t) = \frac{1}{f_d(\boldsymbol{r},\xi,t)}\int_{-\infty}^{+\infty} \boldsymbol{c} m_p p d\Omega \tag{10}$$

$$v_\xi(\boldsymbol{r},\xi,t) = \frac{1}{f_d(\boldsymbol{r},\xi,t)}\int_{-\infty}^{+\infty} \Xi m_p p d\Omega \tag{11}$$

$$\omega_s(\boldsymbol{r},\xi,t) = \frac{1}{f_d(\boldsymbol{r},\xi,t)}\int_{-\infty}^{+\infty} \omega_{s,p} m_p p d\Omega \tag{12}$$

$$T(\boldsymbol{r},\xi,t) = \frac{1}{f_d(\boldsymbol{r},\xi,t)}\int_{-\infty}^{+\infty} T_p m_p p d\Omega \tag{13}$$

$$h(\boldsymbol{r},\xi,t) = \frac{1}{f_d(\boldsymbol{r},\xi,t)}\int_{-\infty}^{+\infty} h_p m_p p d\Omega \tag{14}$$

Peculiar velocity, growth velocity, weight fraction, temperature and enthalpy are defined as the difference between the microscopical and macroscopical velocity and the average of the fluctuation is zero. The pressure tensor and heat flux are defined by:

$$\boldsymbol{P}(\boldsymbol{r},\xi,t) = \int_{-\infty}^{+\infty} m_p \boldsymbol{C}\boldsymbol{C} p d\Omega = f_d\langle \boldsymbol{C}\boldsymbol{C}\rangle \tag{15}$$

$$\boldsymbol{q}(\boldsymbol{r},\xi,t) = \int_{-\infty}^{+\infty} m_p \boldsymbol{C} h' p d\Omega = f_d\langle \boldsymbol{C} h'\rangle \tag{16}$$

We define a space-property pressure vector and a space-property kinetic energy flux as:

$$\boldsymbol{p}_\xi = \int_{-\infty}^{+\infty} m_p v'_\xi \boldsymbol{C} p d\Omega = f_d\langle v'_\xi \boldsymbol{C}\rangle \tag{17}$$

$$q_\xi = \int_{-\infty}^{+\infty} m_p v'_\xi h' p d\Omega = f_d\langle v'_\xi h'\rangle \tag{18}$$

From Equation 2 the equations of change for total mass, species mass, momentum and enthalpy (temperature) are found by inserting for 1, $\omega_{s,p}$, $\boldsymbol{c}$ and h_p for ψ_p, respectively, and applying definitions 10-18.

MODEL DESCRIPTION

Assumptions

With the kinetic theory of gases originally developed for dilute monoatomic gases in vacuum, the application has moved far from the original intentions of the theory, as shown in Figure 3.

The *particles* in this work are bubbles with a significant mass and occupying a significant volume that may vary. The interstitial fluid is a liquid exerting a drag force on the particles and the bubbles are injected into the reactor with an initial velocity, thus not moving freely. The equations are cross-sectionally averaged to reduce the number of spatial dimensions to one. Furthermore, the implemented model is steady-state.

Equations of change

The article presents a novel model particularly designed to described interfacial mass transfer limited chemical processes in a slurry bubble column. The developed equations of change are 3D and transient, but in order to simulate a practical process such as the Fischer-Tropsch synthesis, a reduced 1D steady state model is applied. The developed equations of change are shown below. The population balance equation formulated in terms of a mass density function $f_d(z,\xi)$ is given as:

$$\frac{\partial(f_d(z,\xi)v_z(z,\xi))}{\partial z} + \frac{\partial(f_d(z,\xi)v_\xi(z,\xi))}{\partial \xi} = f_d(z,\xi)\gamma(z,\xi) + J_m(z,\xi) \tag{19}$$

with initial conditions:

$$\begin{aligned} f_d|_{z=z_{\min}} &= f_{d,\text{in}} \\ f_d|_{\xi=\xi_{\min}} &= 0 \end{aligned} \tag{20}$$

In addition, the growth flux $v_\xi f_d$ is set to zero at the ξ boundaries so that no bubbles enter or leave the domain through growth. The growth velocity is defined as Morel (2015), extending it to a density as a function of z and ξ:

$$v_\xi(z,\xi) = -\frac{\xi}{3\rho(z,\xi)}\left[\frac{\partial \rho(z,\xi)}{\partial t} + \boldsymbol{v_r}(z,\xi)\cdot\nabla_r \rho(z,\xi)\right] \tag{21}$$

The continuity equation is subtracted from the equations of change for species mass, momentum and enthalpy (temperature). For the gas phase the dispersion, turbulent dissipation and conduction terms are omitted because the gas phase experiences negligible backmixing. For species mass this gives:

$$\begin{aligned} &v_G(z,\xi)f_d(z,\xi)\frac{\partial \omega_{G,s}(z,\xi)}{\partial z} + v_\xi(z,\xi)f_d(z,\xi)\frac{\partial \omega_{G,s}(z,\xi)}{\partial \xi} \\ &= f_d(z,\xi)\gamma_s(z,\xi) - \omega_s(z,\xi)f_d(z,\xi)\gamma(z,\xi) \\ &+ \langle J_{\omega_{s,p}}\rangle - \omega_s(z,\xi)J_m(z,\xi) \end{aligned} \tag{22}$$

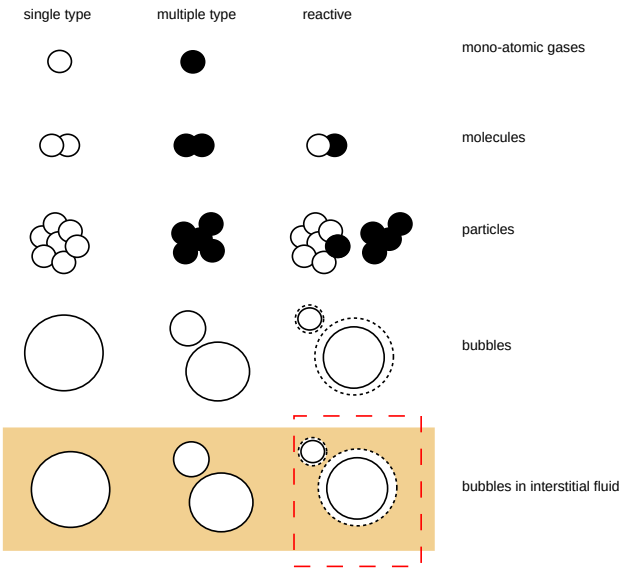

Figure 3: Extension of the subjects to the kinetic theory of gases. The upper left corner represents the origin of kinetic gas theory - a monoatomic gas in a vacuum. Gas atoms of different type, denser gases, particles, bubbles and finally bubbles subject to chemical reactions and in an interstitial fluid, which is considered in this work (inside red dashed line).

The initial conditions are given as:

$$\begin{aligned}\omega_{G,s}|_{z=z_{\min}} &= \omega_{G,s,\text{in}} \\ \omega_{G,s}|_{\xi=\xi_{\min}} &= K_s\omega_{L,s}(z)\end{aligned} \tag{23}$$

The initial condition at $\xi_{\min}$ implies that the smallest bubbles with diameter $\xi_{\min}$ are assumed to be in equilibrium with the liquid phase at all times. For momentum:

$$\begin{aligned}&v_G(z,\xi)f_d(z,\xi)\frac{\partial v_G(z,\xi)}{\partial z} + v_\xi(z,\xi)f_d(z,\xi)\frac{\partial v_G(z,\xi)}{\partial \xi} \\ &= f_d(z,\xi)F_z(z,\xi) + \langle J_{\boldsymbol{c}}\rangle - v_G(z,\xi)J_m(z,\xi)\end{aligned} \tag{24}$$

with the initial conditions:

$$\begin{aligned}v_G|_{z=z_{\min}} &= v_{G,\text{in}} \\ v_G|_{\xi=\xi_{\min}} &= v_L(z)\end{aligned} \tag{25}$$

where the smallest bubbles are assumed to have the same velocity as the liquid. For temperature:

$$\begin{aligned}&c_p v_G(z,\xi)f_d(z,\xi)\frac{\partial T_G(z,\xi)}{\partial z} + c_p v_\xi(z,\xi)f_d(z,\xi)\frac{\partial T_G(z,\xi)}{\partial \xi} \\ &= f_d(z,\xi)q_z(z,\xi) + \langle J_{T_p}\rangle - T_G(z,\xi)J_m(z,\xi)\end{aligned} \tag{26}$$

with initial conditions:

$$\begin{aligned}T_G|_{z=z_{\min}} &= T_{G,\text{in}} \\ T_G|_{\xi=\xi_{\min}} &= T_{SL}(z)\end{aligned} \tag{27}$$

as the smallest bubbles are assumed to have the same temperature as the slurry.

Interfacial transfer terms

Interfacial mass, momentum and heat transfer terms are defined in terms of the size dependent variables weight fraction, velocity and temperature.

Mass transfer

$$f_d(z,\xi)\gamma_s \approx \frac{f_d(z,\xi)A(\xi)k_{L,s}(z)\rho_L}{\rho_G(z,\xi)V(\xi)}\left(\frac{1}{K_s}\omega_{G,s}(z,\xi) - \omega_{L,s}(z)\right) \tag{28}$$

where $A(\xi)$ is the surface area of a bubble, $k_{L,s}(z,\xi)$ is the liquid side mass transfer coefficient, ρ_L is the liquid density (constant in this work), $\omega_{L,s}(z)$ the weight fraction of component s in the liquid phase and K_s an equilibrium constant for component s. The mass transfer term γ is obtained by summing over all s:

$$f_d(z,\xi)\gamma = \sum_s f_d(z,\xi)\gamma_s \tag{29}$$

It is noted that integration of Equation 28 and 29 yield the ξ-averaged mass transfer terms for the liquid phase.

Momentum transfer

The force terms are given by Nayak *et al.* (2011):

$$F_z(z,\xi) = -\frac{f_d(z,\xi)}{\rho_G(z,\xi)}\frac{\partial p(z)}{\partial z} + f_d(z,\xi)g_z + f_{\text{drag}}^{G-L}(z,\xi) \tag{30}$$

where

$$f_{\text{drag}}^{G-L} = -\frac{3}{4}\rho_L\frac{C_D}{\xi}\frac{f_d(z,\xi)}{\rho_G(z,\xi)}|v_G(z,\xi) - v_L(z)|(v_G(z,\xi) - v_L(z)) \tag{31}$$

Integrating Equation 31 over ξ gives the momentum exchange term for use in the liquid phase momentum equation.

Heat transfer

The heat transfer term for heat transfer by convection is similar to the species mass transfer term in mathematical structure:

$$f_d(z,\xi)q_c(z,\xi) = \frac{f_d(z,\xi)A(\xi)h_{G-L}(z,\xi)}{\rho_G(z,\xi)V(\xi)}(T_G(z,\xi) - T_{SL}(z)) \tag{32}$$

Integrating Equation 32 over ξ gives the heat exchange term for use in the slurry temperature equation.

Source terms

The source terms due to coalescence and breakage in the population balance equation (Equation 19) are modelled as:

$$\begin{aligned}&J_m(z,\xi) = -b(\xi)f_d(z,\xi) \\ &+ \rho_G(z,\xi)V(\xi)\int_\xi^{\xi_{max}} h_b(\xi,\zeta)b(\zeta)\frac{f_d(\boldsymbol{r},\zeta,t)}{\rho_G(z,\zeta)V(\zeta)}d\zeta \\ &- f_d(z,\xi)\int_{\xi_{min}}^{(\xi_{max}^3-\xi^3)^{1/3}} c(\xi,\zeta)\frac{f_d(\boldsymbol{r},\zeta,t)}{\rho_G(z,\zeta)V(\zeta)}d\zeta \\ &+ \frac{\xi^2}{2}\rho_G(z,\xi)V(\xi)\int_{\xi_{min}}^{(\xi^3-\xi_{min}^3)^{1/3}} \ldots \\ &\frac{c([\xi^3-\zeta^3]^{1/3},\zeta)f_d(\boldsymbol{r},[\xi^3-\zeta^3]^{1/3},t)f_d(\boldsymbol{r},\zeta,t)}{[\xi^3-\zeta^3]^{2/3}\rho_G(z,\zeta)V(\zeta)\rho_G(z,[\xi^3-\zeta^3]^{1/3})V([\xi^3-\zeta^3]^{1/3})}d\zeta\end{aligned} \tag{33}$$

where the closure models by Coulaloglou and Tavlarides (1977) for breakage frequency and daughter size redistribution are applied. A pre-factor of $K_B = 2\times10^{-3}$ was multiplied to the breakage terms to adjust the resultant breakage frequency to reasonable numbers within the bubble size domain along the axial direction of the reactor. Coalescence was not included in the simulations as bubble column flows generally are breakage dominated Sporleder *et al.* (2011). Breakage and coalescence terms for the species mass, momentum and energy equations are in general not known. As continuity is subtracted from the species mass, momentum and energy equations, two source terms appear in each equation. These are assumed to be equal (but with opposite sign) through the assumption that the product of averages equal to average of products and thus cancel. The result is that only the continuity equation has source terms due to coalescence and breakage.

Liquid and solid phase equations

The liquid and solid phase equations are the standard axial dispersion model equations coupled with a momentum equation for each phase. The solid phase is assumed to have the same temperature as the liquid phase. The liquid and solid phases is collectively referred to as the slurry temperature. No species mass equation is applied for the solid phase. The liquid and solid equations along with Fischer-Tropsch specific reactor parameters are given in Vik *et al.* (2015).

SOLUTION METHOD AND IMPLEMENTATION

The equations of change for species mass, total mass, momentum and enthalpy (temperature) for the dispersed, liquid and solid phases were implemented in MATLAB® and solved using the orthogonal collocation method. 22 points were used in the axial direction and 35 points in the property (diameter) direction. Convergence was taken as when the global iteration error was less than 10^{-5}. The mass loss/gain in the model was calculated for each phase as the difference

between phase specific mass flux entering and leaving the model, divided by the phase specific mass flux entering the reactor.

Operating conditions

The operating conditions are given in Table 1.

Table 1: Operating conditions.

Reactor inlet temperature	T	220 °C
Reactor outlet pressure	p_0	3 MPa
Inlet superficial gas velocity	$v_G^{s,0}$	0.26 m/s
Inlet superficial liquid velocity	$v_L^{s,0}$	0.01 m/s
Dispersion (reactor) height	H	50 m
Reactor diameter	D	9 m
Mass of catalyst per mass of dispersion	α_s	0.05
Product distribution parameter	α_{ASF}	0.9
H_2/CO feed (mole based) ratio	-	2
Liquid density (constant)	ρ_L	687 kg/m^3
Bubble size range	ξ	0.1 -15 mm

RESULTS

Interfacial transfer fluxes

The interfacial fluxes for mass, momentum and energy for a single bubble as defined in Equations 28/29, 31 and 32 are shown in Figures 4, 5 and 6 for bubbles of size 0.1 to 15 mm. Available surface area for a single bubble as function of diameter is shown in Figure 7. Mass and heat flux are directly proportional to the available surface area and this is seen in the left plot of Figures 4 and 6. All three fluxes are inversely proportional to ξ. But as the driving force is squared in the drag force (as opposed to linear in mass and heat flux) the drag force has a different slope than do the mass and heat flux.

The interfacial gas-liquid mass transfer flux occurs as the reaction alters the liquid concentrations and thus gives a driving force between them. The interfacial mass transfer flux reaches a peak as the reaction rate is at its maximum level in the liquid phase.

The interfacial momentum flux is more of a constant magnitude over the axial direction of the reactor. As the bubbles are injected with a high velocity of 0.5 m/s and the liquid phase moves slowly with 0.02 m/s, the gas bubbles are slowed down by the liquid phase along the reactor height.

The interfacial heat transfer flux occurs first with a positive sign (observed from the gas side) as the bubbles are heated by the heat of the reaction in the liquid phase. Then with a negative sign as the liquid is cooled by the installed cooling rods (Figure 1) and successively cools the gas bubbles. The gas-liquid heat flux shows a peak slightly higher in the dispersion than does the mass flux, reflecting the peak of the heat of the reaction. The smaller bubbles have their maximum heating rate slightly lower in the reactor than do the larger bubbles, showing quicker heat transfer due to their higher available surface area for heat transfer.

Size dependent weight fractions

Figure 8 shows the weight fraction of CO as function of bubble size and axial direction. The field value is lower than the average for the smallest bubble sizes and higher for the largest bubble sizes. The largest difference seen between the field value and the average value at the smallest bubble size is 12 wt% units higher for the average than the field. For the largest bubble the field value is up to 8 wt% units lower than the average. The difference is at its largest at the middle of the reactor height (around 25 m). The maximum difference in concentration between the smallest and largest bubble size is 20 wt% units at the middle of the reactor height. CO is the reactant and is thus transported out of the bubble. Smaller bubbles have higher surface area per mass of gas and thus allow for more mass transport. A lower concentration of reactant for the smaller bubbles and vice versa for the large bubbles is thus an expected result.

The main difference between the size dependent model in this work and the average model is the use of a size dependent mass transfer term. A size dependent mass transfer term takes the difference in surface area per bubble gas mass into account and can predict the effect of bubble size on mass transfer. As mentioned above, mass transfer coefficients for the Fischer-Tropsch synthesis are claimed to vary by one order of magnitude. Figure 9 shows the effect of increasing and decreasing the value of the liquid side mass transfer coeffi-

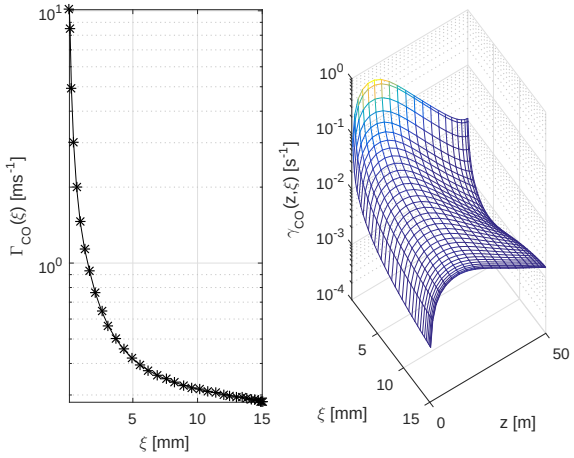

Figure 4: Mass flux of CO for a single bubble as function of bubble size for bubble sizes 0.1 mm to 15 mm. Left: Mass transfer flux for a single bubble integrated over the entire height of the reactor. Right: Mass transfer flux as function of bubble size and axial direction for a single bubble.

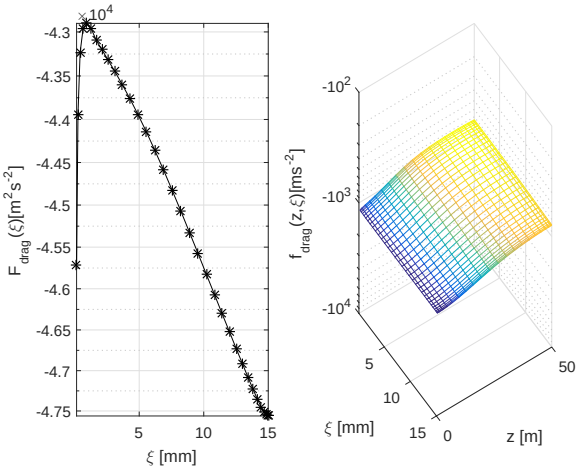

Figure 5: Drag force for a single bubble as function of bubble size for bubble sizes 0.1 mm to 15 mm. Left: Drag force for a single bubble integrated over the entire height of the reactor. Right: Drag force as function of bubble size and axial direction for a single bubble.

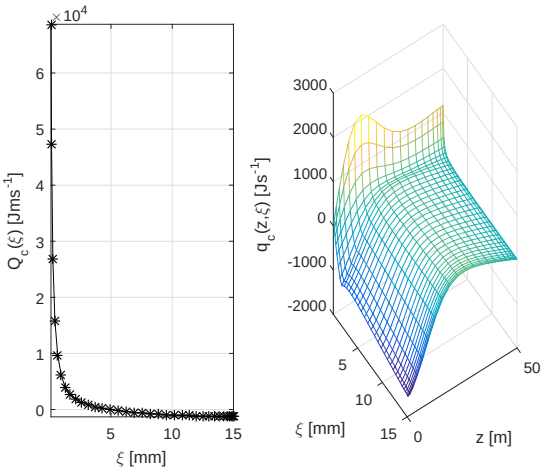

Figure 6: Heat flux for a single bubble as function of bubble size for bubble sizes 0.1 mm to 15 mm. Left: Heat flux for a single bubble integrated over the entire height of the reactor. Right: Heat flux as function of bubble size and axial direction for a single bubble.

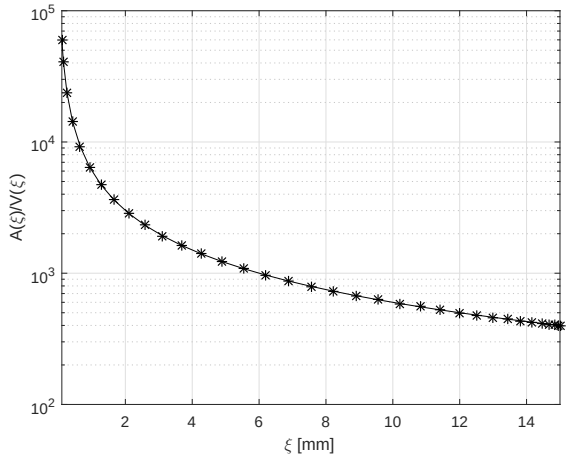

Figure 7: Surface area per volume for bubbles with diameter 0.1 to 15 mm.

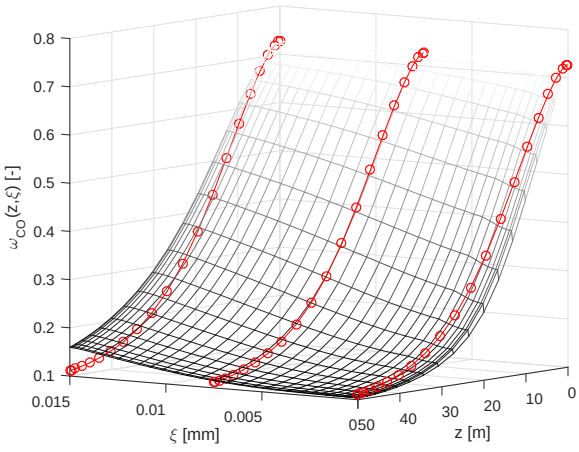

Figure 8: Weight fraction of CO (reactant) as function of bubble size and axial direction. Large bubbles have more reactant left in the bubble than the average. Small bubbles have less reactant left than the average.

cient by one order of magnitude. The nomial conversion at the outlet is 89%. Increasing the mass transfer coefficient by an order of magnitude gives 93%. Decreasing it gives a conversion of 48%. These numbers indicate that the mass transfer coefficient plays a significant role in the Fischer-Tropsch synthesis at the given operating conditions. The process is mass transfer limited at the given catalyst concentration (Table 1).

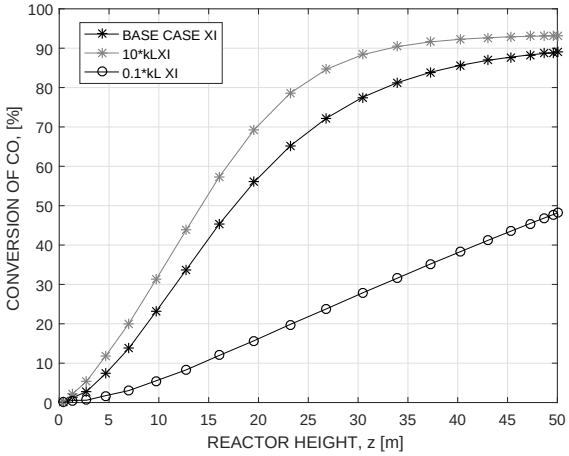

Figure 9: Conversion of CO in wt% as function of axial direction for increase and decrease in the liquid side mass transfer coefficient from the nominal value calculated from the small bubble correlation by Calderbank and Moo-Young (1961). Small k_L value is large mass transfer resistance, high k_L value is low mass transfer resistance. 45 wt% catalyst per volume of slurry.

It is noted that the base case simulation (Table 1) has a high catalyst loading of 45 wt% per volume of slurry. As a sensitivity a set of simulations with a 20 wt% catalyst concentration is given in Figure 10.

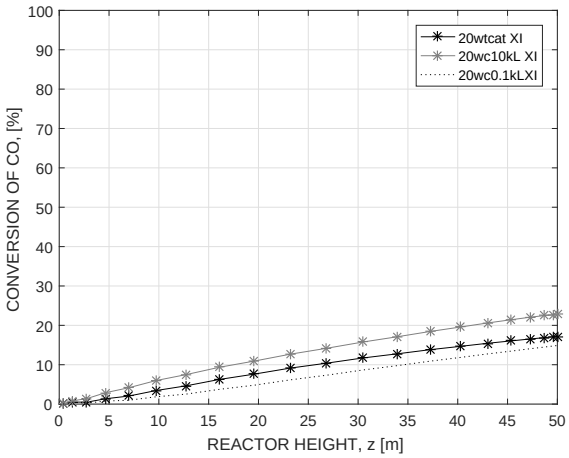

Figure 10: Conversion of CO in wt% as function of axial direction for increase and decrease in the liquid side mass transfer coefficient from the nominal value calculated by the formula from Calderbank and Moo-Young (1961). 20 wt% catalyst per volume of slurry.

The conversion of CO decreases from 89% to 17% for the nominal k_L value. For the tenfold increase, the conversion increases to 23%. For the low k_L value the result is a decrease from to 15%. The difference in conversion between the smallest and largest k_L values is smaller for lower catalyst

concentrations, as is expected. With a lower catalyst concentration it is less likely for the mass transfer to be the limiting resistance in the overall efficiency of the reactor. However, there is a potential to increase reactor efficiency by increasing mass transfer also at lower catalyst concentrations.

A detailed modelling of the mass transfer flux as function of the bubble size requires a good model for k_L, also its dependency on bubble size. Calderbank and Moo-Young (1961) claimed the bubble size of less importance and claimed k_L rather being a function of the liquid properties such as diffusivity than being a function of bubble size. However, the number of experimental studies of mass transfer at high pressures and with high gas flow rates is low (Rollbusch *et al.*, 2015), in particular if also requiring measurements in Fischer-Tropsch-like fluids.

Size dependent velocity

Figure 11 shows the bubble size dependent velocity compared to the mass averaged velocity. For the smallest bubbles the difference is very large; the average is 0.4 to 0.6 m/s and the smallest bubble size in the field value has the same velocity as the liquid (set as boundary condition) of 0.02 m/s. The large variation in velocity as a function of bubble size is dictated by the drag coefficient for a single bubble by Tomiyama (1998). The coefficient is corrected by a factor p; $C_D = C_D'(1-\alpha_G)^p$ to account for bubble interaction. In this work we use the value of 2 Ishii and Zuber (1979). The value of p is further discussed by Rampure *et al.* (2007). It is noted that the value of p is uncertain and has influence on the velocity.

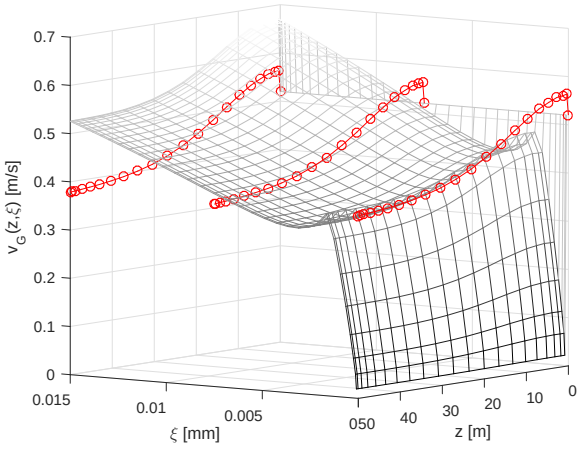

Figure 11: Velocity as function of bubble size ξ and axial direction z. The average value is shown as connected red circles. The difference in the velocity for the smallest and largest bubbles is 0.6 m/s.

Size dependent temperature

Figure 12 shows the temperature as a function of bubble size and axial direction, with average values in red connected circles. The field deviates from the average value by less than 0.02K at all points. The maximal variation in the temperature profile along the axis is 10 K. The size dependency of the temperature is so small that it may be considered negligible for this system. It is noted that the gas and liquid phases are fed at the same temperature in this simulation. In case of difference between gas and liquid inlet temperatures or with lower values for the interfacial heat transfer coefficient the bubble size dependency of the temperature may be important.

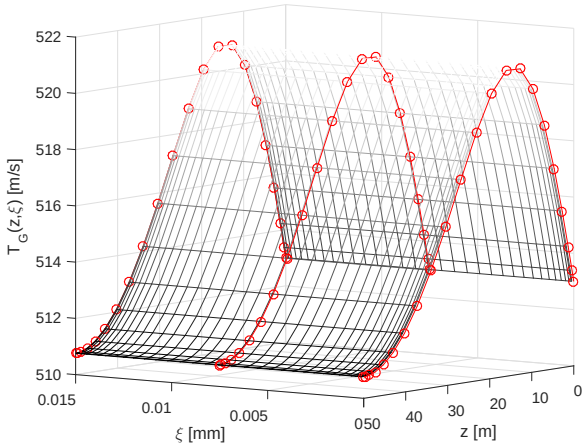

Figure 12: Temperature as function of bubble size ξ and axial direction z. The average value is shown with connected red circles. No variation in temperature as function of bubble size is visible.

Effect of bubble size

A simulation was performed with a mean inlet bubble size of 15 mm instead of 10 mm. The results are shown in Figure 13. With an interfacial area reduced to about 50% of the nominal value, the conversion of CO decreases by 10 wt% points. The gas velocity increases as bigger bubbles are less slowed down by drag than smaller bubbles. The difference in outlet bubble size is shown in the lower left plot in Figure 13 and shows a difference of 8 mm for the peak bubble size. It is noted that the total bubble (gas) mass in the reactor was 9 % less in the sensitivity with a mean bubble size of 15 mm compared to the base case of 10 mm. The total bubble volume was 6 % less.

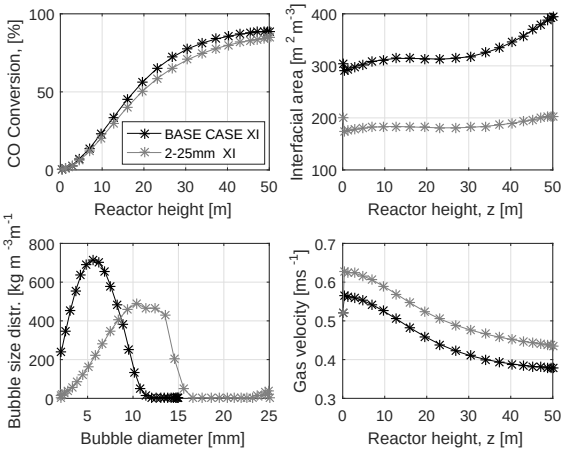

Figure 13: Conversion of CO, interfacial area, bubble size distribution at outlet and gas velocity for a mean inlet bubble size of 10 mm (base case) in black and 15 mm in gray.

CONCLUSION

A bubble size dependent model for weight fractions, velocity and temperature has been developed and applied to the

Fischer-Tropsch synthesis in a slurry bubble column operating at industrial conditions.

The interfacial fluxes are inversely proportional to the bubble diameter and thus decrease with increasing diameter. The consequence is a higher mass, momentum (drag force) and heat transfer rate for the smaller bubbles than for the larger.

Bubble size dependent velocity is known from the literature to give a valuable additional information compared to all bubbles having the same average velocity. This is also true here, as the drag force exerted on small bubbles is very different than for large bubbles resulting in a velocity profile highly dependent on bubble size. The difference in velocity for the smallest and largest bubbles is 0.6 m/s at its maximum which is significant as the average velocity is about 0.45 m/s.

Bubble size dependent weight fractions show a concentration difference between the smallest and largest bubble sizes of maximum 0.2 at the conditions modelled here. With a weight fraction of reactant ranging from 0.1 to 0.7 this is a significant difference. Bubble size dependent weight fractions give more accurate description of the mass transfer in a reactor, given a proper k_L value for the system, preferably as a function of bubble size. This poses a challenge as k_L as a function of bubble size is difficult to measure at industrial conditions such high pressure, high temperature and multicomponent viscous hydrocarbon fluids.

Bubble size dependent temperature does not add significant information new in the process studied here. The temperature as function of bubble size is relatively flat and the maximal deviation for any bubble size from the average temperature is 0.02 K. It is noted that the gas and liquid phases are fed at the same temperature in this simulation. In case of difference between gas and liquid inlet temperatures or with lower values for the interfacial heat transfer coefficient the bubble size dependency of the temperature may be important.

Given that mass transfer influences the overall conversion in the reactor, it is important to model this interfacial flux with the necessary level of detail. A bubble size dependent transfer flux combined with the information in the explicit density function $f_d(z,\xi)$ provides a good starting point to increase the level of detail in modelling mass transfer in mass transfer limiting chemical and biochemical processes. It is noted that firm conclusions on the mass and heat transfer limitations can only be drawn when reliable estimates of the transfer coefficients are available.

REFERENCES

ANDRESEN, E. (1990). *Statistical Approach to Continuum Models for Turbulent Gas-Particle Flows*. Ph.D. thesis, Technical University of Denmark.

CALDERBANK, P.H. and MOO-YOUNG, M.B. (1961). "The continous phase heat and mass-transfer properties of dispersions". *Chemical Engineering Science*, **16**, 39–54.

CHAO, Z. (2012). *Modeling and Simulatino of Reactive Three-phase FLows in Fluidized Bed Reactors Application to the SE-SMR Process*. Ph.D. thesis, Norwegian University of Science and Technology (NTNU).

COULALOGLOU, C. and TAVLARIDES, L. (1977). "Description of interaction processes in agitated liquid-liquid dispersions". *Chem. Eng. Sci.*, **(30)**, 1289–1297.

DORAO, C.A. (2006). *High Order Methods for the Solution of the Population Balance Equation with Applications to Bubbly Flows*. Ph.D. thesis, Norwegian University of Science and Technology (NTNU).

FRANK, T., ZWART, P.J., SHI, J.M., KREPPER, E., LUCAS, D. and ROHDE, U. (2005). "Inhomogeneous musig model - a population balance approach for polydispersed bubbly flows". *International Conference, Nuclear Energy for New Europe 2005*.

ISHII, M. and ZUBER, N. (1979). "Drag coefficient and relative velocity in bubbly, droplet or particulate flows". *AIChE Journal*, **25**, 843–855.

JAKOBSEN, H.A. (2008). *Chemical Reactor Modeling Multiphase Reactive Flows*. Springer.

KOHLER, M.A. (1986). "Comparison of mechanically agitated and bubble column slurry reactors". *Applied Catalysis*, **22**, 21–53.

LATHOUWERS, D. and BELLAN, J. (2000). "Modeling of dense gas-solid reactive mixtures applied to biomass pyrolysis in a fluidized bed". *Proceedings of the 2000 U.S. DOE Hydrogen Program Review NREL/CP-570-28890*.

MOREL, C. (2015). *Mathematical Modeling of Disperse Two-Phase Flows*. Springer International Publishing Switzerland.

NAYAK, A., BORKA, Z., PATRUNO, L., SPORLEDER, F., DORAO, C. and JAKOBSEN, H. (2011). "A combined multifluid-population balance model for vertical gas-liquid bubble-driven flows considering bubble column operating conditions". *Ind. Eng. Chem. Res.*, **50(3)**, 1786–1798.

PATRUNO, L.E., DORAO, C.A., DUPUY, P.M., SVENDSEN, H.F. and JAKOBSEN, H.A. (2009). "Identification of droplet breakage kernel for population balance modelling". *Chemical Engineering Science*, **64**, 638–645.

RAMPURE, M.R., KULKARNI, A.A. and RANADE, V.V. (2007). "Hydrodynamics of bubble column reactors at high gas velocity Experiments and computational fluid dynamics (cfd) simulations". *Industrial & Engineering Chemical Research*, 8431–8447.

ROLLBUSCH, P., BOTHE, M., BECKER, M., LUDWIG, M., GRÜNEWALD, M., SCHLÜTER, M. and FRANKE, R. (2015). "Bubble columns operated under industrial relevant conditions - current understanding of design parameters". *Chemical Engineering Science*.

SIMONIN, O. (1996). "Continuum modelling of dispersed two-phase flows". *Combustion and turbulence in two-phase flows*, vol. 2, 1–47. van Karman Institute for fluid dynamics.

SOLSVIK, J. and JAKOBSEN, H.A. (2014). "A combined multifluid-population balance model applied to dispersed gas-liquid flows". *Journal for Dispersion Science and Technology*.

SPORLEDER, F. (2011). *Simulation of Chemical Reactors using the Least-Squares Spectral Element Method*. Ph.D. thesis, Norwegian University of Science and Technology (NTNU).

SPORLEDER, F., DORAO, C.A. and JAKOBSEN, H.A. (2011). "Model based on population balance for the simulation of bubble columns using methods of the least-square type". *Chemical Engineering Science*, **66**, 3133–3144.

TOMIYAMA, A. (1998). "Struggle with computational bubble dynamics". *Multiphase Science and Technology*, **10(4)**, 369–405.

VANDU, C., KOOP, K. and KRISHNA, R. (2004). "Volumetric mass transfer coefficient in a slurry bubble column operating in the heterogeneous flow regime". *Chemical Engineering Science*, 4516–5423.

VIK, C.B., SOLSVIK, J., HILLESTAD, M. and JAKOBSEN, H.A. (2015). "Modeling of a slurry bubble column reactor for the production of biofuels via the fischer-tropsch synthesis". *Chemical Engineering & Technology*, **38(4)**, 690–700. URL `http://dx.doi.org/10.`

1002/ceat.201400647.

YATES, I.C. and SATTERFIELD, C.N. (1991). "Intrinsic kinetics of the fischer-tropsch synthesis on a cobalt catalyst". *Energy & Fuels*, **5(1)**, 168–173.

ZHU, Z. (2009). *The Least-Squares Spectral Element Method Solution of the Gas-Liquid Multi-fluid Model Coupled with the Population Balance Equation*. Ph.D. thesis, Norwegian University of Science and Technology (NTNU).